

Exploring Heavy Higgs Bosons at a 100 TeV Hadron Collider within the Semi-Constrained NMSSM

Kun Wang,^{1,*} Pengfu Tian,² and Jingya Zhu^{3,†}

¹College of Science, University of Shanghai for Science and Technology, Shanghai 200093, China

²School of Physics and Technology, Wuhan University, Wuhan 430072, China

³School of Physics and Electronics, Henan University, Kaifeng 475004, China

(Dated: April 19, 2024)

In this study, we explore the detectability of heavy Higgs bosons in the $pp \rightarrow b\bar{b}H/A \rightarrow b\bar{b}t\bar{t}$ channel at a 100 TeV hadron collider within the semi-constrained Next-to-Minimal Supersymmetric Standard Model (NMSSM). We calculate their production cross sections and decay branching ratios, comparing these with simulation results from existing reference. We focus on the heavy, doublet-dominated CP-even Higgs H and CP-odd Higgs A , with mass limits set below 10 TeV to ensure detectability. We find that at a collider with 3 ab^{-1} of integrated luminosity, the potential for detecting heavy Higgs bosons varies significantly with their mass and $\tan\beta$. Heavy Higgs bosons below 2 TeV are within the testable range, while those heavier than 7 TeV fall below the exclusion and discovery thresholds, rendering them undetectable. For masses between 2 and 7 TeV, heavy Higgs bosons with $\tan\beta$ less than 20 can be detected, whereas those with $\tan\beta$ greater than 20 are beyond the current discovery or exclusion capabilities.

I. INTRODUCTION

It has been widely acknowledged for an extended period that the Standard Model (SM) of particle physics, despite its remarkable success in explaining a vast array of phenomena, fails to provide a complete description of the fundamental aspects of the universe. Consequently, the search for new physics beyond the SM (BSM) has become a crucial direction in modern physics research.

The discovery of a Higgs boson with properties consistent with SM predictions at the Large Hadron Collider (LHC) in 2012 significantly bolstered our understanding of the SM [1–4]. Nevertheless, this milestone also intensified the debate regarding the possible existence of additional Higgs bosons. These scalar particles are theoretically predicted by a large number of natural BSM models, which aim to address the limitations and unresolved questions of the SM. Among these are the Minimal Supersymmetric Standard Model (MSSM) [5–16], the Next-to-MSSM (NMSSM) [17–33], the Minimal Dilaton Model (MDM) [34–38], and the Little Higgs Models (LHM) [39, 40], among others. The experimental search for heavy neutral Higgs bosons has focused on decay channels such as $\tau^+\tau^-$ [41, 42], $t\bar{t}$, $b\bar{b}$, $\mu^+\mu^-$, ZZ , WW , hh , and hV , which are reviewed in [43, 44]. And recently evidence for a new scalar around 151 GeV was accumulated with significances of 4.3σ local and 3.9σ global [45], subsequently revised to 4.1σ locally and 3.5σ globally [46].

The exploration of new physics phenomena, especially the detection of heavy Higgs bosons, requires colliders with higher energy. Future high-energy colliders, designed to exceed the capabilities of current facilities,

will be able to examine these heavy particles. Notably, the Future hadron-hadron Circular Collider (FCC-hh) at CERN [47] and the Super- pp -Collider (SppC) [48, 49] in China are among the most ambitious projects in this direction. Both initiatives aim to construct a 50-100 TeV pp collider [50], promising a significant leap in the energy frontier and potentially uncovering phenomena beyond the SM. Moreover, the concept of a multi-TeV muon collider presents an innovative approach to high-energy physics experiments [51, 52]. Extensive research has been conducted on the detection of heavy Higgs bosons at future colliders. In particular, the studies described in Ref. [53] examined the $pp \rightarrow b\bar{b}H/A \rightarrow b\bar{b}\tau\tau$ and $pp \rightarrow b\bar{b}H/A \rightarrow b\bar{b}t\bar{t}$ channels at a 100 TeV pp collider, and proposed pushing the exclusion limits for heavy Higgs searches up to $M_H \sim 10$ TeV, with exceptions in regions of low $\tan\beta$. Furthermore, the analysis in Ref. [13] explored the $pp \rightarrow H/A \rightarrow \tilde{\chi}_1^0 \tilde{\chi}_2^\mp$ process, revealing the $4\ell + \cancel{E}$ signal at a 100 TeV hadron collider, demonstrating its ability to probe new supersymmetric model sectors. In addition, Ref. [54] explored the potential of a multi-TeV muon collider to discover heavy Higgs bosons within Two Higgs Doublet Models (2HDMs) and assess the discriminative power among different 2HDM types.

In the current study, we extend the investigation initiated in our previous work on heavy Higgs bosons within the framework of the semi-constrained NMSSM (scNMSSM) [55]. The NMSSM incorporates an additional singlet superfield to the MSSM, thereby enriching the Higgs and neutralino sectors. Our analysis focuses on the computational evaluation of production cross sections and decay branching ratios for these heavy Higgs bosons. Through these calculations, we aim to provide a comprehensive understanding of the behavior and detectability of heavy Higgs bosons within the scNMSSM. Furthermore, we delve into the exploration of the discovery potential of these heavy Higgs bosons through the $pp \rightarrow b\bar{b}H/A \rightarrow b\bar{b}t\bar{t}$ channel at a future 100 TeV col-

* kwang@usst.edu.cn

† zhuji@henu.edu.cn

lider. The selection of a 100 TeV collider is driven by its exceptional ability to achieve the high energy levels required for producing such massive particles, thus opening up new avenues for their discovery.

The remainder of this manuscript is organized as follows. In Sec. II, we provide a brief overview of the scNMSSM, outlining its fundamental aspects and theoretical significance. In Sec. III, we present a detailed account of our computational methodology, followed by a comprehensive discussion of the results obtained from our analysis. In Sec. IV, we conclude the paper by summarizing the main results and their implications for future research in this area.

II. THE SEMI-CONSTRAINED NMSSM

The NMSSM extends the MSSM by introducing an additional singlet superfield, denoted as \hat{S} , where the superpotential of the \mathbb{Z}_3 -symmetric NMSSM is defined as:

$$W_{\text{NMSSM}} = W_{\text{MSSM}}|_{\mu=0} + \lambda \hat{S} \hat{H}_u \cdot \hat{H}_d + \frac{\kappa}{3} \hat{S}^3, \quad (1)$$

where $W_{\text{MSSM}}|_{\mu=0}$ is the superpotential of the MSSM without the μ -term, λ and κ are coupling constants, \hat{H}_u and \hat{H}_d are the doublet Higgs superfields, and \hat{S} is the added singlet superfield. After electroweak symmetry breaking, the singlet scalar's vacuum expectation value (VEV), denoted v_s , dynamically generates the massive μ -term [56, 57]

$$\mu \equiv \lambda v_s. \quad (2)$$

Concurrently, the scalar components H_u and H_d also attain VEVs, labeled v_u and v_d , respectively. This leads to the introduction of a new parameter $\tan \beta$, defined as

$$\tan \beta \equiv v_u/v_d, \quad (3)$$

where the sum of their squares is $v_u^2 + v_d^2 = v^2 = (174 \text{ GeV})^2$.

The NMSSM introduces specific soft SUSY breaking terms, distinct from those in the MSSM, as given by:

$$-\mathcal{L}_{\text{NMSSM}}^{\text{soft}} = -\mathcal{L}_{\text{MSSM}}^{\text{soft}}|_{\mu=0} + m_S^2 |S|^2 + \lambda A_\lambda S H_u \cdot H_d + \frac{1}{3} \kappa A_\kappa S^3 + \text{h.c.}, \quad (4)$$

where $\mathcal{L}_{\text{MSSM}}^{\text{soft}}|_{\mu=0}$ denotes the MSSM's soft SUSY breaking terms with the μ parameter set to zero. The symbols H_u and H_d refer to the scalar components of the Higgs doublets, A_λ and A_κ represent the trilinear coupling constants with mass dimension, and m_S is the mass of the singlet scalar field.

In the scNMSSM, the Higgs sector is allowed to deviate from universality at the Grand Unified Theory (GUT) scale, a characteristic also known as the NMSSM with non-universal Higgs masses. Specifically, the soft masses for the Higgs fields, $m_{H_u}^2$, $m_{H_d}^2$, and m_S^2 , can differ from

$M_0^2 + \mu^2$. Furthermore, the trilinear coupling constants A_λ and A_κ may vary independently from A_0 . Consequently, the parameter space of the scNMSSM is defined by nine parameters:

$$\lambda, \kappa, \tan \beta, \mu, A_\lambda, A_\kappa, A_0, M_{1/2}, M_0. \quad (5)$$

Here, $M_{1/2}$ and M_0 represent the universal sfermion mass and the universal gaugino mass, respectively, while A_0 denotes the universal trilinear coupling constant in the sfermion sector.

The Higgs sector within the NMSSM is predicted to contain three CP-even Higgs bosons, two CP-odd Higgs bosons, and a pair of charged Higgs bosons. For convenience, the scalar components of the superfields H_u , H_d , and S are often rotated so that they can be represented as

$$H_1 = \cos \beta H_u + \varepsilon \sin \beta H_d^* = \begin{pmatrix} H^+ \\ \frac{S_1 + iP_1}{\sqrt{2}} \end{pmatrix}, \quad (6)$$

$$H_2 = \sin \beta H_u - \varepsilon \cos \beta H_d^* = \begin{pmatrix} G^+ \\ v + \frac{S_2 + iG^0}{\sqrt{2}} \end{pmatrix}, \quad (7)$$

$$H_3 = S = v_s + \frac{S_3 + iP_2}{\sqrt{2}}, \quad (8)$$

where $\varepsilon = \begin{pmatrix} 0 & 1 \\ -1 & 0 \end{pmatrix}$, and S_1 , S_2 , and S_3 create the CP-even basis, while P_1 and P_2 establish the CP-odd one. H_2 is identified as the SM-like Higgs, H_1 represents a new Higgs doublet field, and H_3 introduces a new singlet field.

The CP-even Higgs mass matrix M_S^2 in the basis (S_1, S_2, S_3) is given by [21, 58]:

$$M_{S,11}^2 = M_A^2 + (m_Z^2 - \lambda^2 v^2) \sin^2 2\beta, \quad (9)$$

$$M_{S,12}^2 = -\frac{1}{2} (m_Z^2 - \lambda^2 v^2) \sin 4\beta, \quad (10)$$

$$M_{S,13}^2 = -\left(\frac{M_A^2}{2\mu/\sin 2\beta} + \kappa v_s \right) \lambda v \cos 2\beta, \quad (11)$$

$$M_{S,22}^2 = m_Z^2 \cos^2 2\beta + \lambda^2 v^2 \sin^2 2\beta, \quad (12)$$

$$M_{S,23}^2 = 2\lambda\mu v \left[1 - \left(\frac{M_A}{2\mu/\sin 2\beta} \right)^2 - \frac{\kappa}{2\lambda} \sin 2\beta \right], \quad (13)$$

$$M_{S,33}^2 = \frac{1}{4} \lambda^2 v^2 \left(\frac{M_A}{\mu/\sin 2\beta} \right)^2 + \kappa v_s A_\kappa + 4(\kappa v_s)^2 - \frac{1}{2} \lambda \kappa v^2 \sin 2\beta, \quad (14)$$

where M_A is defined as:

$$M_A = \frac{2\mu(A_\lambda + \kappa v_s)}{\sin 2\beta}. \quad (15)$$

The CP-odd Higgs mass matrix M_P^2 in the basis (P_1, P_2) is given by:

$$M_{P,11}^2 = M_A^2, \quad (16)$$

$$M_{P,12}^2 = \lambda v (A_\lambda - 2\kappa v_s), \quad (17)$$

$$M_{P,22}^2 = \lambda (A_\lambda + 4\kappa v_s) \frac{v_u v_d}{v_s} - 3\kappa v_s A_\kappa. \quad (18)$$

Three CP-even mass eigenstates h_1, h_2 , and h_3 ($m_{h_1} < m_{h_2} < m_{h_3}$) are derived from the mixture of (S_1, S_2, S_3) , and two CP-odd mass eigenstates a_1 and a_2 ($m_{a_1} < m_{a_2}$) are derived from (P_1, P_2) . This can be represented as:

$$\begin{pmatrix} h_1 \\ h_2 \\ h_3 \end{pmatrix} = S_{ij} \begin{pmatrix} S_1 \\ S_2 \\ S_3 \end{pmatrix}, \quad (19)$$

$$\begin{pmatrix} a_1 \\ a_2 \end{pmatrix} = P_{ij} \begin{pmatrix} P_1 \\ P_2 \end{pmatrix}, \quad (20)$$

where S_{ij} and P_{ij} are the mixing matrices that diagonalize the mass matrices M_S^2 and M_P^2 , respectively.

Among the three CP-even Higgs bosons (h_i , where $i = 1, 2, 3$), the 125 GeV SM-like Higgs could be either h_1 or h_2 , both of which are predominantly doublet-dominated scalars. The remaining CP-even Higgs bosons include another doublet-dominated and a singlet-dominated scalar. For the two CP-odd Higgs bosons (a_i , where $i = 1, 2$), one is doublet-dominated, and the other is singlet-dominated. The singlet-dominated Higgs boson rarely couples to fermions because the singlet S interacts only with the Higgs sector. This property makes it difficult to detect at the LHC. In contrast, the doublet-dominated Higgs boson couples to fermions, which facilitates its detection. Our study focuses only on the heavy, doublet-dominated CP-even Higgs H and CP-odd Higgs A , because of their detectability. The couplings to up/down-type fermions of these heavy Higgs bosons, H and A , are defined as follows:

$$C_{Huu}^{SUSY} = i \frac{m_u}{v} \cot \beta \quad (21)$$

$$C_{Hdd}^{SUSY} = i \frac{m_d}{v} \tan \beta \quad (22)$$

$$C_{Auu}^{SUSY} = \frac{m_u}{v} \cot \beta \gamma_5 \quad (23)$$

$$C_{Add}^{SUSY} = \frac{m_d}{v} \tan \beta \gamma_5 \quad (24)$$

The reduced couplings of these heavy Higgs bosons, H and A , are defined as follows:

$$C_{Huu} = C_{Huu}^{SUSY} / C_{Huu}^{SM} = \cot \beta \quad (25)$$

$$C_{Auu} = C_{Auu}^{SUSY} / C_{Auu}^{SM} = \cot \beta \quad (26)$$

$$C_{Hdd} = C_{Hdd}^{SUSY} / C_{Hdd}^{SM} = \tan \beta \quad (27)$$

$$C_{Add} = C_{Add}^{SUSY} / C_{Add}^{SM} = \tan \beta \quad (28)$$

Furthermore, it is observed that when $\tan \beta$ is significantly larger than 1 ($\tan \beta \gg 1$), $M_{S,11}^2$ closely approximates M_A^2 . In addition, the Higgs bosons H and A become degenerate, meaning they have the same mass and exhibit identical couplings to quarks.

III. RESULTS AND DISCUSSIONS

In this study, we explore the detectability of the heavy, doublet-dominated CP-even Higgs (H) and CP-odd Higgs (A) in the scNMSSM, at a 100 TeV Hadron

Collider. We set the upper mass limit for the Higgs at 10 TeV, represented as:

$$h_i, a_j < 10 \text{ TeV} \quad \text{for } i = 1, 2, 3; j = 1, 2. \quad (29)$$

Therefore, we consider the relevant parameter space in the scNMSSM as follows:

$$0.0 < \lambda < 0.7, \quad |\kappa| < 0.7, \quad 1 < \tan \beta < 60,$$

$$0.0 < \mu, M_0, M_{1/2} < 10 \text{ TeV},$$

$$|A_0|, |A_\lambda|, |A_\kappa| < 10 \text{ TeV}.$$

We use the package `NMSSMTools-6.0.2` [59–62] to scan the parameter space and calculate relevant quantities, considering the following constraints: (i) Theoretical constraints including vacuum stability and without Landau pole below the GUT scale [59, 60]. (ii) Flavor constraints from rare B-meson decays and D -meson mass differences [63–66]. (iii) A 123–127 GeV Higgs boson with signal predictions that are globally consistent with LHC Higgs data [3, 4, 67–71]. (iv) Constraints from searches for additional Higgs bosons and exotic decays of the SM-like Higgs, using `HiggsBounds-5.5.0`, including a limit of 10.7% on invisible Higgs decay [72–77]. (v) Upper bounds on the dark matter relic density from WMAP/Planck [78, 79]. (vi) Direct dark matter search constraints from XENON1T [80, 81], PICO-60 [82], PandaX-4T [83, 84] and LUX-ZEPLIN [85]. (vii) Constraints from direct SUSY searches at the LHC and LEP, using the package `SModelS-v2.2.1` [86–92].

For the samples satisfying the above theoretical and experimental constraints, we observe the following properties:

- The squarks of the first two generations are heavier than 2.2 TeV, with the lightest squark, \tilde{t}_1 , exceeding 1 TeV.
- The third-generation sleptons can be as light as approximately 170 GeV.
- The gluino mass exceeds 2 TeV. Consequently, given the universal gaugino mass condition at the GUT scale, the bino and wino masses are more than 340 GeV and 620 GeV, respectively.
- The mass range for the lightest neutralino varies from 4 GeV to 4 TeV, typically dominated by bino and singlino compositions, with some higgsino admixture.
- In the Higgs sector, we categorize the samples into two types:
 - h_1 is the 125 GeV SM-like Higgs. h_2 and h_3 are heavy CP-even Higgs bosons, while a_1 and a_2 are heavy CP-odd Higgs bosons.
 - h_2 is the 125 GeV SM-like Higgs. The light CP-even Higgs h_1 and the light CP-odd Higgs a_1 are typically singlet-dominant. The heavy CP-even Higgs h_3 and the light CP-odd Higgs a_2 are typically doublet-dominant.

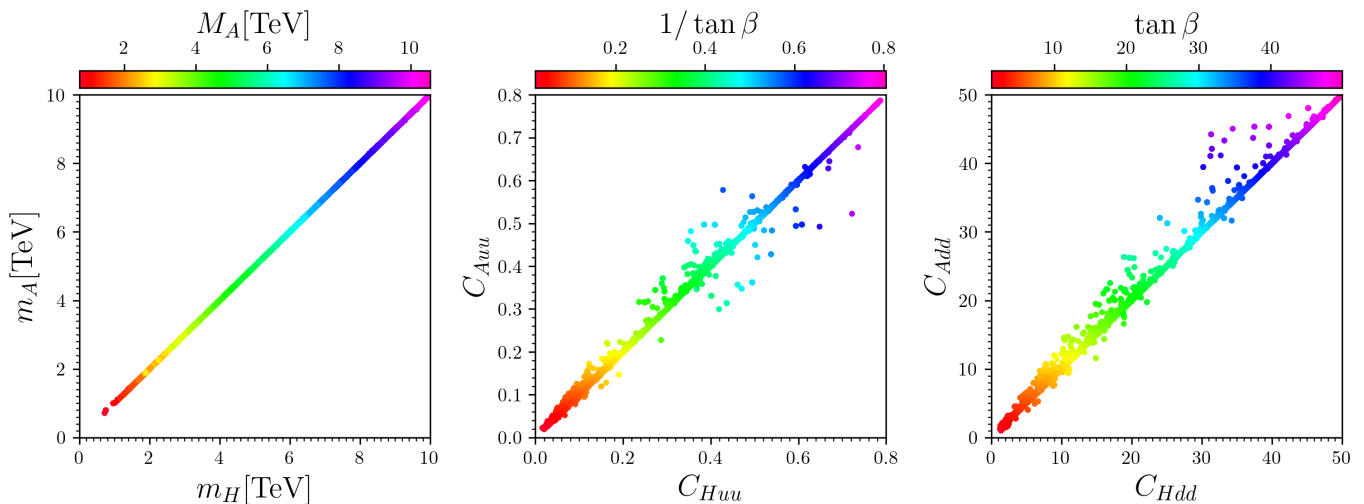


FIG. 1. Surviving samples are shown in the planes of m_A versus m_H (left), reduced coupling C_{Auu} versus C_{Huu} (middle), and reduced coupling C_{Add} versus C_{Hdd} (right). From left to the right, the colors represent M_A , $1/\tan\beta$, and $\tan\beta$ respectively. Samples with larger values of $\tan\beta$ are plotted on top of those with smaller values.

In this study, we focus on doublet-dominant heavy Higgs due to the difficulty of detecting singlet-dominant Higgs. There are two types to consider. In the first type, h_1 resembles the SM-like Higgs, with either h_2 or h_3 being doublet-dominant, and the same holds for a_1 and a_2 , where one of them is doublet-dominant. We label the heavy CP-even and CP-odd doublet-dominant Higgs as H and A , respectively. In the second type, h_2 acts as the SM-like Higgs, with h_3 and a_2 typically being doublet-dominant, also denoted as H and A . Thus, H and A represent the heavy CP-even and CP-odd doublet-dominant Higgs in subsequent discussions. For the heavy Higgs H and A , which have masses ranging from 0.6 TeV to 10 TeV, we calculate their production cross sections and decay branching ratios. We also compare the $pp \rightarrow bbH \rightarrow bbt\bar{t}$ signal with simulation results found in Ref. [53].

In Fig. 1, we show the mass and reduced coupling of the heavy doublet-dominated Higgs bosons H and A in the scNMSSM. The following observations can be made from these figures:

- In the left panel, the surviving samples are plotted on the m_A versus m_H plane, with colors indicating M_A . It is observed that H and A have nearly identical masses, approximately equal to the parameter M_A . This similarity arises because, according to Eq. 16, P_1 is the CP-odd doublet-dominated Higgs, and since A is also denoted as the CP-odd doublet-dominated Higgs, it follows that $m_A \approx M_A$. Furthermore, S_1 is the CP-even doublet-dominated Higgs, labeled here as H . From Eq. 9, when $\tan\beta \gg 1$, it is derived that $m_H \approx M_A$. And the mass of H and A is between 0.6 TeV and 10 TeV.
- In the middle panel, the surviving samples are displayed on the plane of reduced coupling with up-

type fermions for A versus H , with the colors indicating $1/\tan\beta$. It is evident that for most samples, C_{Auu} and C_{Huu} are approximately equal to $1/\tan\beta$. This approximation arises because the doublet components of H and A are neither exactly equal nor exactly equal to 1. Furthermore, the values of the reduced couplings C_{Huu} and C_{Auu} range from 0 to 0.8.

- In the right panel, the surviving samples are plotted on the plane of reduced coupling with down-type fermions for A versus H , with colors representing $\tan\beta$. The results are similar to those in the middle panel; for most samples, C_{Add} and C_{Hdd} approximate $\tan\beta$. This approximation is also due to the doublet components of H and A not being exactly equal or exactly equal to 1. Additionally, the values of the reduced couplings C_{Hdd} and C_{Add} vary from 0 to 50.

In Fig. 2 we show the decay properties of the CP-even doublet-dominated heavy Higgs H in the scNMSSM, with colors representing $\tan\beta$. Since both heavy Higgs A and H are doublet-dominated, their couplings to fermions show very little difference. The only difference is that $Br(A \rightarrow VV/\tilde{V}\tilde{V}) = 0$. However, this difference is minimal due to the small coefficient $C_{HV\tilde{V}}$. As a consequence, the decay properties of the CP-odd doublet-dominated heavy Higgs A are very similar to those of H ; therefore, the plot for A is omitted. The following observations can be drawn from these plots:

- The dominant branching ratios consistently arise from the decays to $t\bar{t}$, $b\bar{b}$ and SUSY particles, with these branching ratios reaching values close to 1.
- In the upper left panel, the branching ratio of H to $t\bar{t}$ is inversely proportional to $\tan\beta$; that is, the

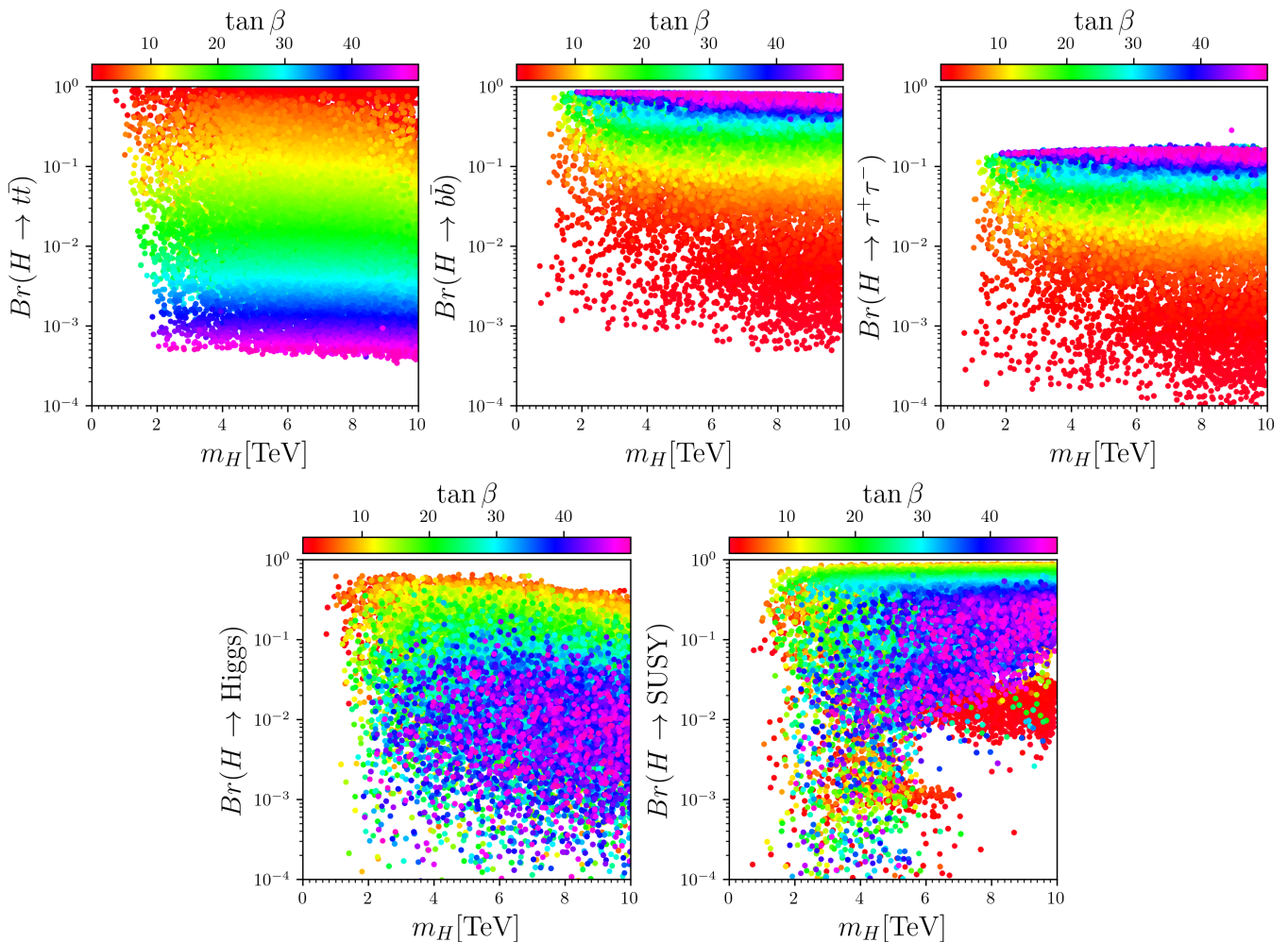


FIG. 2. Surviving samples in the planes of branching ratios versus m_H , with colors representing $\tan\beta$. The branching ratios pertain to the decays of the heavy CP-even Higgs H into $t\bar{t}$, $b\bar{b}$, $\tau^+\tau^-$, all possible lighter Higgs bosons, and all possible SUSY particles, respectively. Samples with larger values of $\tan\beta$ are plotted on top of those with smaller values.

smaller the $\tan\beta$, the larger the branching ratio $Br(H \rightarrow t\bar{t})$. This relationship is due to C_{Huu} being directly proportional to $1/\tan\beta$. Consequently, when $\tan\beta < 10$, the branching ratio $Br(H \rightarrow t\bar{t})$ exceeds 0.2. As $\tan\beta$ approaches 1, the branching ratio $Br(H \rightarrow t\bar{t})$ tends towards 1.

- In the upper middle and right panels, the branching ratios of H to $b\bar{b}$ and $\tau^+\tau^-$ are proportional to $\tan\beta$; specifically, the larger the $\tan\beta$, the higher the branching ratios $Br(H \rightarrow b\bar{b})$ and $Br(H \rightarrow \tau^+\tau^-)$. This proportionality is due to C_{Hdd} being directly proportional to $\tan\beta$. Additionally, when $\tan\beta$ exceeds 40, the maximum branching ratio $Br(H \rightarrow b\bar{b})$ can reach up to 0.8, while the maximum branching ratio $Br(H \rightarrow \tau^+\tau^-)$ can only reach up to 0.2. Furthermore, the branching ratio $Br(H \rightarrow \tau^+\tau^-)$ is generally lower than $Br(H \rightarrow b\bar{b})$ due to the lower mass of τ compared to b , as the coupling strength of Higgs with fermions

is proportional to their mass.

- In the lower left panel, the branching ratios of H to light Higgs bosons are relatively small, reaching a maximum of approximately 0.6. Additionally, for samples where $\tan\beta$ exceeds 40, the maximum branching ratio $Br(H \rightarrow \text{light Higgs})$ is only 0.1.
- In the lower right panel, the maximum branching ratios of H to SUSY particles can approach 0.8. Additionally, it is observed that when $\tan\beta$ ranges from 10 to 30, the branching ratios $Br(H \rightarrow \text{SUSY})$ can approach this maximum value of 0.8, remaining above 0.5. When $\tan\beta$ is less than 10, the heavy Higgs H predominantly decays into $t\bar{t}$; conversely, when $\tan\beta$ exceeds 30, it primarily decays into $b\bar{b}$.

We calculate the cross sections for the process $pp \rightarrow b\bar{b}H$ in the SM with m_H ranging from 0.5 to 10 TeV at $\sqrt{s} = 100$ TeV using MG5_aMC_v2.6.7 [93, 94]. The calculated cross section for m_H or m_A in our samples

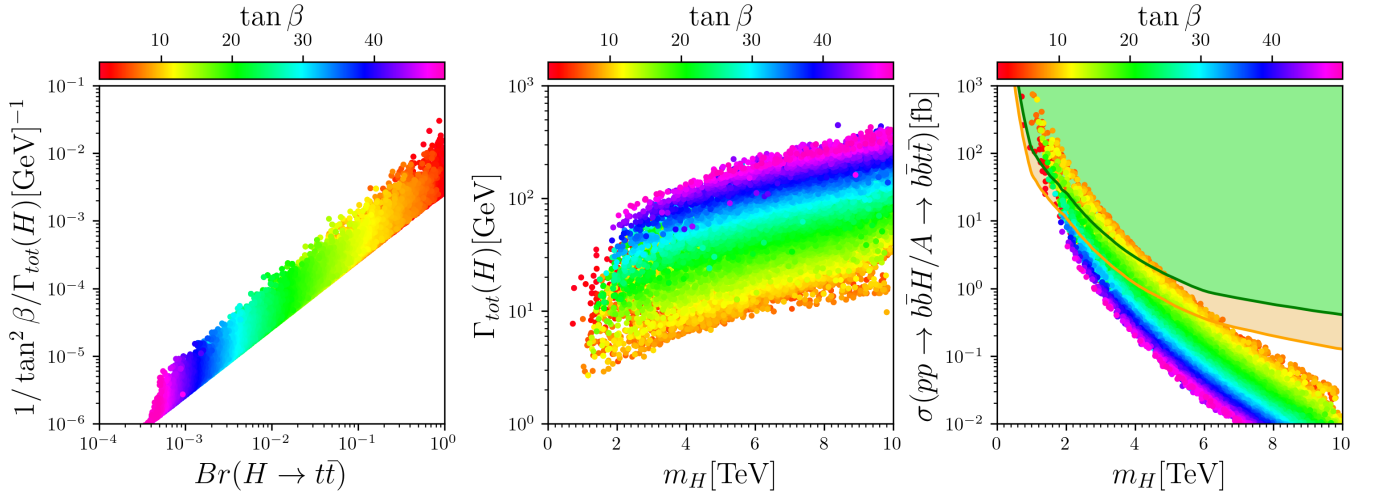


FIG. 3. Surviving samples are shown in the planes of $1/\tan^2\beta/\Gamma_{tot}(H)$ versus $Br(H \rightarrow t\bar{t})$ (left), heavy Higgs total decay width $\Gamma_{tot}(H)$ versus heavy Higgs mass m_H (middle), and cross section of $pp \rightarrow b\bar{b}H/A \rightarrow b\bar{b}t\bar{t}$ versus heavy Higgs mass m_H (right), where the colors of the samples indicate $\tan\beta$. The red and green curves represent the model-independent exclusion and discovery ranges, respectively, for the $pp \rightarrow b\bar{b}H/A \rightarrow b\bar{b}t\bar{t}$ channel, with an integrated luminosity of 3 ab^{-1} at 100 TeV, as taken from Fig.9 in Ref. [53]. Samples with larger values of $\tan\beta$ are plotted on top of those with smaller values.

is multiplied by the square of the reduced coupling C_{Hbb} and the branching ratio $Br(H/A \rightarrow t\bar{t})$. Since the masses and various couplings of the heavy Higgs H and A are very similar, along with nearly identical branching ratios $Br(H \rightarrow t\bar{t})$ and $Br(A \rightarrow t\bar{t})$, and similar reduced couplings C_{Hbb} and C_{Abb} , the heavy Higgs bosons H and A are considered degenerate in the detection channel $pp \rightarrow b\bar{b}H/A \rightarrow b\bar{b}t\bar{t}$. Therefore, the cross section for the $pp \rightarrow b\bar{b}H/A \rightarrow b\bar{b}t\bar{t}$ channel is twice that of the individual H or A channels. Production rates for our samples in the $pp \rightarrow b\bar{b}H/A \rightarrow b\bar{b}t\bar{t}$ channel are presented in the left panel of Fig. 3, where colors indicate $\tan\beta$. The red and green curves represent the model-independent exclusion and discovery reaches, respectively, with an integrated luminosity of 3 ab^{-1} at 100 TeV, as depicted in Fig.9 of Ref. [53]. In calculating the SM cross section, we employed both the four-flavor scheme (4FS) and five-flavor scheme (5FS) cross sections [95], and combined them using the formula from Ref. [96]:

$$\sigma = \frac{\sigma^{4\text{FS}} + \omega\sigma^{5\text{FS}}}{1 + \omega}, \quad (30)$$

where $\omega = \ln(m_H/m_b) - 2$.

In Fig. 3 we show the cross section for the $pp \rightarrow b\bar{b}H/A \rightarrow b\bar{b}t\bar{t}$ channel of the CP-even doublet-dominated heavy Higgs H/A in the scNMSSM, with colors representing $\tan\beta$. Since the heavy Higgs A and H are considered degenerate, the cross section $\sigma(pp \rightarrow b\bar{b}H/A \rightarrow b\bar{b}t\bar{t}) = 2\sigma(pp \rightarrow b\bar{b}H \rightarrow b\bar{b}t\bar{t})$. The following observations can be drawn from these plots:

- In the left panel, $1/\tan^2\beta/\Gamma_{tot}(H)$ appears to be directly proportional to $Br(H \rightarrow t\bar{t})$. This is because the decay diagram for $Br(H \rightarrow t\bar{t})$ includes

a coupling vertex C_{Huu} , and when calculating the decay cross-section, a C_{Huu}^2 term is introduced. Thus, $Br(H \rightarrow t\bar{t})$ is proportional to $1/\tan^2\beta$. Additionally, the branching ratio $Br(H \rightarrow t\bar{t})$ is inversely proportional to the total decay width $\Gamma_{tot}(H)$, which is represented as:

$$Br(H \rightarrow t\bar{t}) = \frac{\sigma(H \rightarrow t\bar{t})}{\Gamma_{tot}(H)} \sim \frac{1/\tan^2\beta}{\Gamma_{tot}(H)}. \quad (31)$$

- In the middle panel, the total decay width $\Gamma_{tot}(H)$ of the heavy Higgs increases exponentially with $\tan\beta$. Additionally, when $\tan\beta$ remains constant, $\Gamma_{tot}(H)$ increases with the mass of the heavy Higgs m_H .
- In the right panel, the cross section $\sigma(pp \rightarrow b\bar{b}H/A \rightarrow b\bar{b}t\bar{t})$ decreases rapidly as the mass of the heavy Higgs m_H increases. The cross section for $pp \rightarrow b\bar{b}H \rightarrow b\bar{b}t\bar{t}$ can be approximated as follows:

$$\begin{aligned} & \sigma(pp \rightarrow b\bar{b}H \rightarrow b\bar{b}t\bar{t}) \\ & \approx \sigma(pp \rightarrow b\bar{b}H^{SM}) \cdot C_{Hdd}^2 \cdot Br(H \rightarrow t\bar{t}) \\ & \approx \frac{\sigma(pp \rightarrow b\bar{b}H^{SM})}{\Gamma_{tot}(H)} \end{aligned} \quad (32)$$

This decline is because $\sigma(pp \rightarrow b\bar{b}H \rightarrow b\bar{b}t\bar{t})$ is proportional to $\sigma(pp \rightarrow b\bar{b}H^{SM})$, and the production cross section $\sigma(pp \rightarrow b\bar{b}H^{SM})$ diminishes with an increase in mass. It can also be observed that samples with smaller $\tan\beta$ values have larger cross sections $\sigma(pp \rightarrow b\bar{b}H \rightarrow b\bar{b}t\bar{t})$. This is because $\sigma(pp \rightarrow b\bar{b}H \rightarrow b\bar{b}t\bar{t})$ is inversely proportional to the total decay width $\Gamma_{tot}(H)$, and $\Gamma_{tot}(H)$ exponentially increases as $\tan\beta$ increases.

- In the right panel, the regions above the green and red curves indicate where the samples can be covered by 2σ and 5σ , respectively, with an integrated luminosity of 3 ab^{-1} at 100 TeV. This implies that through the $pp \rightarrow b\bar{b}H/A \rightarrow b\bar{b}t\bar{t}$ channel in the scNMSSM, samples with a heavy Higgs mass $m_H < 2\text{ TeV}$ can be tested at the 100 TeV collider with 3 ab^{-1} of integrated luminosity. For samples with the heavy Higgs mass $m_H > 7\text{ TeV}$, they fall below the exclusion and discovery curves, thus they cannot be discovered or excluded. Samples with the heavy Higgs mass in the range of $2-7\text{ TeV}$ and $\tan\beta < 20$ can be tested at the 100 TeV collider with 3 ab^{-1} of integrated luminosity.

In Table I, we present four benchmark samples detailing the Higgs sector, where $\sigma(X)$ represents the cross section $\sigma(pp \rightarrow b\bar{b}X \rightarrow b\bar{b}t\bar{t})$. The heavy Higgs bosons H and A , corresponding to h_3 and a_2 respectively, are doublet-dominated, while S_{33}^2 and P_{22}^2 indicate the singlet components in H and A . We find that H and A have minimal singlet components, suggesting that h_2 and a_1 are primarily singlet-dominated. Due to their weak coupling to fermions, these singlet-dominated bosons, h_2 and a_1 , are difficult to detect at colliders.

IV. CONCLUSION

In this study, we explore the potential for detecting heavy Higgs bosons in the $pp \rightarrow b\bar{b}H/A \rightarrow b\bar{b}t\bar{t}$ channel at a 100 TeV hadron collider within the semi-constrained NMSSM. First, we scan the relevant parameter space with the NMSSMTools package, which includes theoretical constraints such as vacuum stability and Landau poles, as well as experimental constraints like Higgs data, B physics, sparticle searches, dark matter relic density, and direct detection experiments. We observe that singlet-dominated Higgs bosons S are difficult to detect due to their limited interactions outside the Higgs sector. Therefore, our analysis primarily focuses on the more detectable heavy, doublet-dominated CP-even Higgs H and CP-odd Higgs A , limiting their masses to below 10 TeV to remain detectable. The presence of a CP-even Higgs (h_1 or h_2) resembling the 125 GeV SM-like Higgs does not affect these findings. Since that the heavy Higgs H and A are nearly identical in mass and couplings, the cross section for the combined channel $pp \rightarrow b\bar{b}H/A \rightarrow b\bar{b}t\bar{t}$ is effectively double that of the single H channel.

We calculated their decay branching ratios and production rates, and compared these with the simulation results cited in Ref. [53]. Finally, we draw the following conclusions about the heavy Higgs bosons A and H , with masses ranging from 0.6 to 10 TeV, in the semi-constrained NMSSM:

- When the heavy Higgs bosons are doublet-dominated, their reduced couplings with up-type fermions, C_{Huu} and C_{Auu} , are approximately equal

TABLE I. Four Benchmark Points for Surviving Samples, where $\sigma(X)$ denotes the cross section $\sigma(pp \rightarrow b\bar{b}X \rightarrow b\bar{b}t\bar{t})$. Here, H and A represent the doublet-dominated heavy Higgs bosons, while S_{33}^2 and P_{22}^2 indicate the singlet components in H and A respectively.

	P1	P2	P3	P4
λ	0.61	0.21	0.10	0.10
κ	0.36	-0.21	-0.42	0.67
$\tan\beta$	2.07	4.98	20.02	47.91
μ [GeV]	361	345	295	498
M_0 [GeV]	8072	1506	5811	9596
M_{12} [GeV]	3402	5569	3017	9289
A_0 [GeV]	7306	-6275	539	9862
A_λ [GeV]	4961	1230	4983	2357
A_κ [GeV]	2720	252	3769	-3588
m_{h_1} [GeV]	124	124	124	125
m_{h_2} [GeV]	341	648	1942	6796
m_H [GeV]	720	2025	4030	7950
m_{a_1} [GeV]	512	277	2920	1860
m_A [GeV]	716	2026	4031	7950
S_{31}^2	0.99	1.00	1.00	1.00
S_{32}^2	0.00	0.00	0.00	0.00
S_{33}^2	0.01	0.00	0.00	0.00
P_{21}^2	1.00	1.00	1.00	1.00
P_{22}^2	0.00	0.00	0.00	0.00
C_{h_2uu}	0.1	0.0	0.0	0.0
C_{Huu}	-0.5	-0.2	-0.1	0.0
C_{a_1uu}	0.0	0.0	0.0	0.0
C_{Auu}	0.5	0.2	0.0	0.0
C_{h_2dd}	0.4	0.1	0.0	0.3
C_{Hdd}	2.0	5.0	20.0	47.9
C_{a_1dd}	0.0	-0.2	-0.3	0.1
C_{Add}	2.1	5.0	20.0	47.9
$Br(h_2 \rightarrow t\bar{t})$	0	0.01	4.4×10^{-4}	7.9×10^{-8}
$Br(H \rightarrow t\bar{t})$	0.87	0.41	0.01	5.7×10^{-4}
$Br(a_1 \rightarrow t\bar{t})$	0.95	0	6.0×10^{-5}	2.6×10^{-7}
$Br(A \rightarrow t\bar{t})$	0.91	0.41	0.01	5.7×10^{-4}
$\Gamma_{tot}(h_2)$ [GeV]	0.20	0.39	0.65	59.04
$\Gamma_{tot}(H)$ [GeV]	7.71	8.99	45.27	236.25
$\Gamma_{tot}(a_1)$ [GeV]	4.8×10^{-4}	1.2×10^{-4}	1.08	0.59
$\Gamma_{tot}(A)$ [GeV]	8.93	9.12	45.31	236.33
$\sigma(h_2)$ [fb]	0	0.01	1.6×10^{-6}	4.3×10^{-11}
$\sigma(H)$ [fb]	331.80	16.80	0.29	2.9×10^{-3}
$\sigma(a_1)$ [fb]	0.10	0.00	1.7×10^{-6}	5.8×10^{-9}
$\sigma(A)$ [fb]	360.03	16.73	0.29	2.9×10^{-3}

to $1/\tan\beta$. This relationship causes the branching ratio of H/A to $t\bar{t}$ to be inversely proportional to $\tan\beta$; specifically, a smaller $\tan\beta$ results in a larger branching ratio $Br(H \rightarrow t\bar{t})$. Conversely, the reduced couplings with down-type fermions, C_{Hdd} and C_{Add} , approximate to $\tan\beta$, leading to branching ratios of H to $b\bar{b}$ and $\tau^+\tau^-$ that are directly proportional to $\tan\beta$.

- When $\tan\beta$ is less than 10, the heavy Higgs H predominantly decays into $t\bar{t}$, with the branching ratio $Br(H \rightarrow t\bar{t})$ reaching up to 1. When $\tan\beta$ exceeds 30, it primarily decays into $b\bar{b}$, with the branching

ratio $Br(H \rightarrow b\bar{b})$ up to 0.8 and $Br(H \rightarrow \tau^+\tau^-)$ also reaching up to 0.2. For $\tan\beta$ values between 10 and 30, the branching ratio $Br(H \rightarrow SUSY)$ is dominant, reaching up to 0.8.

- The branching ratio $Br(H \rightarrow t\bar{t})$ is proportional to $1/\tan^2\beta$ and inversely proportional to the total decay width $\Gamma_{\text{tot}}(H)$. Furthermore, the total decay width of the heavy Higgs, $\Gamma_{\text{tot}}(H)$, increases exponentially with $\tan\beta$.
- The cross section $\sigma(pp \rightarrow b\bar{b}H/A \rightarrow b\bar{b}t\bar{t})$ decreases rapidly as the mass of the heavy Higgs (m_H) increases, and it is inversely proportional to the total decay width $\Gamma_{\text{tot}}(H)$. Consequently, this cross section also decreases exponentially with increasing $\tan\beta$.
- For the $pp \rightarrow b\bar{b}H/A \rightarrow b\bar{b}t\bar{t}$ channel at a 100 TeV collider with 3 ab^{-1} of integrated luminosity in the semi-constrained NMSSM:

- Heavy Higgs bosons with a mass $m_H < 2 \text{ TeV}$ can be tested.
- Heavy Higgs bosons with a mass $m_H > 7 \text{ TeV}$ fall below the exclusion and discovery thresholds, and therefore cannot be discovered or excluded.
- For heavy Higgs masses in the range of 2-7 TeV, those with $\tan\beta \lesssim 20$ can be tested, while those with $\tan\beta \gtrsim 20$ cannot be discovered or excluded.

ACKNOWLEDGMENTS

This work was supported by the National Natural Science Foundation of China (NNSFC) under grant Nos. 12275066 and 11605123.

-
- [1] G. Aad *et al.* (ATLAS), *Phys. Lett. B* **716**, 1 (2012), [arXiv:1207.7214 \[hep-ex\]](#).
- [2] S. Chatrchyan *et al.* (CMS), *Phys. Lett. B* **716**, 30 (2012), [arXiv:1207.7235 \[hep-ex\]](#).
- [3] G. Aad *et al.* (ATLAS), *Nature* **607**, 52 (2022), [Erratum: *Nature* 612, E24 (2022)], [arXiv:2207.00092 \[hep-ex\]](#).
- [4] A. Tumasyan *et al.* (CMS), *Nature* **607**, 60 (2022), [Erratum: *Nature* 623, (2023)], [arXiv:2207.00043 \[hep-ex\]](#).
- [5] A. D. Medina and M. A. Schmidt, *JHEP* **08**, 095 (2017), [arXiv:1706.04994 \[hep-ph\]](#).
- [6] P. Bechtle, H. E. Haber, S. Heinemeyer, O. Stål, T. Stefaniak, G. Weiglein, and L. Zeune, *Eur. Phys. J. C* **77**, 67 (2017), [arXiv:1608.00638 \[hep-ph\]](#).
- [7] R. K. Barman, B. Bhattacharjee, A. Chakraborty, and A. Choudhury, *Phys. Rev. D* **94**, 075013 (2016), [arXiv:1607.00676 \[hep-ph\]](#).
- [8] M. Carena, J. Ellis, J. S. Lee, A. Pilaftsis, and C. E. M. Wagner, *JHEP* **02**, 123 (2016), [arXiv:1512.00437 \[hep-ph\]](#).
- [9] A. Djouadi and J. Quevillon, *JHEP* **10**, 028 (2013), [arXiv:1304.1787 \[hep-ph\]](#).
- [10] P. Bechtle, S. Heinemeyer, O. Stal, T. Stefaniak, G. Weiglein, and L. Zeune, *Eur. Phys. J. C* **73**, 2354 (2013), [arXiv:1211.1955 \[hep-ph\]](#).
- [11] H. Baer, V. Barger, X. Tata, and K. Zhang, *Symmetry* **15**, 548 (2023), [arXiv:2212.09198 \[hep-ph\]](#).
- [12] U. Chattopadhyay, A. Datta, S. Mukherjee, and A. K. Swain, *JHEP* **08**, 113 (2022), [arXiv:2201.00621 \[hep-ph\]](#).
- [13] H. Baer, C. Kao, V. Barger, R. Jain, D. Sengupta, and X. Tata, *Phys. Rev. D* **105**, 095039 (2022), [arXiv:2112.02232 \[hep-ph\]](#).
- [14] H. Bahl, P. Bechtle, S. Heinemeyer, S. Liebler, T. Stefaniak, and G. Weiglein, *Eur. Phys. J. C* **80**, 916 (2020), [arXiv:2005.14536 \[hep-ph\]](#).
- [15] A. Adhikary, S. Banerjee, R. Kumar Barman, and B. Bhattacharjee, *JHEP* **09**, 068 (2019), [arXiv:1812.05640 \[hep-ph\]](#).
- [16] P. S. Bhupal Dev and A. Pilaftsis, *JHEP* **12**, 024 (2014), [Erratum: *JHEP* 11, 147 (2015)], [arXiv:1408.3405 \[hep-ph\]](#).
- [17] S. Ma, K. Wang, and J. Zhu, *Chin. Phys. C* **45**, 023113 (2021), [arXiv:2006.03527 \[hep-ph\]](#).
- [18] L. Shang, P. Sun, Z. Heng, Y. He, and B. Yang, *Eur. Phys. J. C* **80**, 574 (2020).
- [19] J. Cao, X. Guo, Y. He, P. Wu, and Y. Zhang, *Phys. Rev. D* **95**, 116001 (2017), [arXiv:1612.08522 \[hep-ph\]](#).
- [20] F. Wang, W. Wang, L. Wu, J. M. Yang, and M. Zhang, *Int. J. Mod. Phys. A* **32**, 1745005 (2017), [arXiv:1512.08434 \[hep-ph\]](#).
- [21] M. Carena, H. E. Haber, I. Low, N. R. Shah, and C. E. M. Wagner, *Phys. Rev. D* **93**, 035013 (2016), [arXiv:1510.09137 \[hep-ph\]](#).
- [22] N.-E. Bomark, S. Moretti, S. Munir, and L. Roszkowski, *JHEP* **02**, 044 (2015), [arXiv:1409.8393 \[hep-ph\]](#).
- [23] J. Cao, D. Li, L. Shang, P. Wu, and Y. Zhang, *JHEP* **12**, 026 (2014), [arXiv:1409.8431 \[hep-ph\]](#).
- [24] S. F. King, M. Mühlleitner, R. Nevzorov, and K. Walz, *Phys. Rev. D* **90**, 095014 (2014), [arXiv:1408.1120 \[hep-ph\]](#).
- [25] J. Baglio, R. Gröber, M. Mühlleitner, D. T. Nhung, H. Rzehak, M. Spira, J. Streicher, and K. Walz, *Comput. Phys. Commun.* **185**, 3372 (2014), [arXiv:1312.4788 \[hep-ph\]](#).
- [26] J.-J. Cao, Z.-X. Heng, J. M. Yang, Y.-M. Zhang, and J.-Y. Zhu, *JHEP* **03**, 086 (2012), [arXiv:1202.5821 \[hep-ph\]](#).
- [27] J. Cao, Z. Heng, J. M. Yang, and J. Zhu, *JHEP* **10**, 079 (2012), [arXiv:1207.3698 \[hep-ph\]](#).
- [28] J. Cao, F. Ding, C. Han, J. M. Yang, and J. Zhu, *JHEP* **11**, 018 (2013), [arXiv:1309.4939 \[hep-ph\]](#).
- [29] Z. Heng, X. Li, and L. Shang, (2023), [arXiv:2308.04822 \[hep-ph\]](#).
- [30] E. Arganda, V. Martín-Lozano, A. D. Medina, and N. I. Mileo, *Adv. High Energy Phys.* **2022**, 2569290 (2022), [arXiv:2102.02290 \[hep-ph\]](#).

- [31] W. Li, H. Qiao, K. Wang, and J. Zhu, (2023), [arXiv:2312.17599 \[hep-ph\]](#).
- [32] K. Wang and J. Zhu, *Chin. Phys. C* **47**, 013107 (2023), [arXiv:2112.14576 \[hep-ph\]](#).
- [33] W. Li, H. Qiao, K. Wang, and J. Zhu, (2023), [arXiv:2312.17523 \[hep-ph\]](#).
- [34] J. Cao, L. Shang, W. Su, Y. Zhang, and J. Zhu, *Eur. Phys. J. C* **76**, 239 (2016), [arXiv:1601.02570 \[hep-ph\]](#).
- [35] B. Agarwal, J. Isaacson, and K. A. Mohan, *Phys. Rev. D* **94**, 035027 (2016), [arXiv:1604.05328 \[hep-ph\]](#).
- [36] J. Cao, Y. He, P. Wu, M. Zhang, and J. Zhu, *JHEP* **01**, 150 (2014), [arXiv:1311.6661 \[hep-ph\]](#).
- [37] L. Liu, H. Qiao, K. Wang, and J. Zhu, *Chin. Phys. C* **43**, 023104 (2019), [arXiv:1812.00107 \[hep-ph\]](#).
- [38] K. Wang and J. Zhu, (2024), [arXiv:2402.11232 \[hep-ph\]](#).
- [39] X.-F. Han, L. Wang, J. M. Yang, and J. Zhu, *Phys. Rev. D* **87**, 055004 (2013), [arXiv:1301.0090 \[hep-ph\]](#).
- [40] K. Cheung, S.-P. He, Y.-n. Mao, P.-Y. Tseng, and C. Zhang, *Phys. Rev. D* **98**, 075023 (2018), [arXiv:1809.03809 \[hep-ph\]](#).
- [41] A. M. Sirunyan *et al.* (CMS), *JHEP* **09**, 007 (2018), [arXiv:1803.06553 \[hep-ex\]](#).
- [42] M. Aaboud *et al.* (ATLAS), *JHEP* **01**, 055 (2018), [arXiv:1709.07242 \[hep-ex\]](#).
- [43] P. A. Zyla *et al.* (Particle Data Group), *PTEP* **2020**, 083C01 (2020).
- [44] M. Aaboud *et al.* (ATLAS), *Phys. Rev. D* **98**, 052008 (2018), [arXiv:1808.02380 \[hep-ex\]](#).
- [45] A. Crivellin, Y. Fang, O. Fischer, S. Bhattacharya, M. Kumar, E. Malwa, B. Mellado, N. Rapheeha, X. Ruan, and Q. Sha, *Phys. Rev. D* **108**, 115031 (2023), [arXiv:2109.02650 \[hep-ph\]](#).
- [46] A. Fowlie, *Phys. Lett. B* **827**, 136936 (2022), [arXiv:2109.13426 \[hep-ph\]](#).
- [47] M. Bicer *et al.* (TLEP Design Study Working Group), *JHEP* **01**, 164 (2014), [arXiv:1308.6176 \[hep-ex\]](#).
- [48] J. Gao, *Int. J. Mod. Phys. A* **36**, 2142005 (2021).
- [49] M. Dong *et al.* (CEPC Study Group), (2018), [arXiv:1811.10545 \[hep-ex\]](#).
- [50] I. Hinchliffe, A. Kotwal, M. L. Mangano, C. Quigg, and L.-T. Wang, *Int. J. Mod. Phys. A* **30**, 1544002 (2015), [arXiv:1504.06108 \[hep-ph\]](#).
- [51] N. Bartosik *et al.*, *JINST* **15**, P05001 (2020), [arXiv:2001.04431 \[hep-ex\]](#).
- [52] M. M. Alsharoa *et al.* (Neutrino Factory, Muon Collider), *Phys. Rev. ST Accel. Beams* **6**, 081001 (2003), [arXiv:hep-ex/0207031](#).
- [53] J. Hajer, Y.-Y. Li, T. Liu, and J. F. H. Shiu, *JHEP* **11**, 124 (2015), [arXiv:1504.07617 \[hep-ph\]](#).
- [54] T. Han, S. Li, S. Su, W. Su, and Y. Wu, *Phys. Rev. D* **104**, 055029 (2021), [arXiv:2102.08386 \[hep-ph\]](#).
- [55] K. Wang and J. Zhu, *JHEP* **06**, 078 (2020), [arXiv:2002.05554 \[hep-ph\]](#).
- [56] U. Ellwanger, C. Hugonie, and A. M. Teixeira, *Phys. Rept.* **496**, 1 (2010), [arXiv:0910.1785 \[hep-ph\]](#).
- [57] M. Maniatis, *Int. J. Mod. Phys. A* **25**, 3505 (2010), [arXiv:0906.0777 \[hep-ph\]](#).
- [58] D. J. Miller, R. Nevzorov, and P. M. Zerwas, *Nucl. Phys. B* **681**, 3 (2004), [arXiv:hep-ph/0304049](#).
- [59] U. Ellwanger, J. F. Gunion, and C. Hugonie, *JHEP* **02**, 066 (2005), [arXiv:hep-ph/0406215](#).
- [60] U. Ellwanger and C. Hugonie, *Comput. Phys. Commun.* **175**, 290 (2006), [arXiv:hep-ph/0508022](#).
- [61] U. Ellwanger and C. Hugonie, *Comput. Phys. Commun.* **177**, 399 (2007), [arXiv:hep-ph/0612134](#).
- [62] D. Das, U. Ellwanger, and A. M. Teixeira, *Comput. Phys. Commun.* **183**, 774 (2012), [arXiv:1106.5633 \[hep-ph\]](#).
- [63] M. Tanabashi *et al.* (Particle Data Group), *Phys. Rev. D* **98**, 030001 (2018).
- [64] R. Aaij *et al.* (LHCb), *Phys. Rev. Lett.* **110**, 021801 (2013), [arXiv:1211.2674 \[hep-ex\]](#).
- [65] J. P. Lees *et al.* (BaBar), *Phys. Rev. Lett.* **109**, 101802 (2012), [arXiv:1205.5442 \[hep-ex\]](#).
- [66] J. P. Lees *et al.* (BaBar), *Phys. Rev. Lett.* **109**, 191801 (2012), [arXiv:1207.2690 \[hep-ex\]](#).
- [67] G. Aad *et al.* (ATLAS), *Phys. Rev. D* **101**, 012002 (2020), [arXiv:1909.02845 \[hep-ex\]](#).
- [68] A. M. Sirunyan *et al.* (CMS), *Eur. Phys. J. C* **79**, 421 (2019), [arXiv:1809.10733 \[hep-ex\]](#).
- [69] G. Aad *et al.* (ATLAS, CMS), *JHEP* **08**, 045 (2016), [arXiv:1606.02266 \[hep-ex\]](#).
- [70] A. M. Sirunyan *et al.* (CMS), *Eur. Phys. J. C* **79**, 421 (2019), [arXiv:1809.10733 \[hep-ex\]](#).
- [71] G. Aad *et al.* (ATLAS, CMS), *JHEP* **08**, 045 (2016), [arXiv:1606.02266 \[hep-ex\]](#).
- [72] P. Bechtel, S. Heinemeyer, O. Stal, T. Stefaniak, and G. Weiglein, *Eur. Phys. J. C* **75**, 421 (2015), [arXiv:1507.06706 \[hep-ph\]](#).
- [73] P. Bechtel, O. Brein, S. Heinemeyer, O. Stål, T. Stefaniak, G. Weiglein, and K. E. Williams, *Eur. Phys. J. C* **74**, 2693 (2014), [arXiv:1311.0055 \[hep-ph\]](#).
- [74] P. Bechtel, O. Brein, S. Heinemeyer, O. Stal, T. Stefaniak, G. Weiglein, and K. Williams, *PoS CHARGED2012*, 024 (2012), [arXiv:1301.2345 \[hep-ph\]](#).
- [75] P. Bechtel, O. Brein, S. Heinemeyer, G. Weiglein, and K. E. Williams, *Comput. Phys. Commun.* **182**, 2605 (2011), [arXiv:1102.1898 \[hep-ph\]](#).
- [76] P. Bechtel, O. Brein, S. Heinemeyer, G. Weiglein, and K. E. Williams, *Comput. Phys. Commun.* **181**, 138 (2010), [arXiv:0811.4169 \[hep-ph\]](#).
- [77] G. Aad *et al.* (ATLAS), *Phys. Lett. B* **842**, 137963 (2023), [arXiv:2301.10731 \[hep-ex\]](#).
- [78] G. Hinshaw *et al.* (WMAP), *Astrophys. J. Suppl.* **208**, 19 (2013), [arXiv:1212.5226 \[astro-ph.CO\]](#).
- [79] P. A. R. Ade *et al.* (Planck), *Astron. Astrophys.* **571**, A16 (2014), [arXiv:1303.5076 \[astro-ph.CO\]](#).
- [80] E. Aprile *et al.* (XENON), *Phys. Rev. Lett.* **121**, 111302 (2018), [arXiv:1805.12562 \[astro-ph.CO\]](#).
- [81] E. Aprile *et al.* (XENON), *Phys. Rev. Lett.* **122**, 141301 (2019), [arXiv:1902.03234 \[astro-ph.CO\]](#).
- [82] C. Amole *et al.* (PICO), *Phys. Rev. D* **100**, 022001 (2019), [arXiv:1902.04031 \[astro-ph.CO\]](#).
- [83] Z. Huang *et al.* (PandaX), *Phys. Lett. B* **834**, 137487 (2022), [arXiv:2208.03626 \[hep-ex\]](#).
- [84] Y. Meng *et al.* (PandaX-4T), *Phys. Rev. Lett.* **127**, 261802 (2021), [arXiv:2107.13438 \[hep-ex\]](#).
- [85] J. Aalbers *et al.* (LZ), *Phys. Rev. Lett.* **131**, 041002 (2023), [arXiv:2207.03764 \[hep-ex\]](#).
- [86] S. Kraml, S. Kulkarni, U. Laa, A. Lessa, W. Magerl, D. Proschofsky-Spindler, and W. Waltenberger, *Eur. Phys. J. C* **74**, 2868 (2014), [arXiv:1312.4175 \[hep-ph\]](#).
- [87] F. Ambrogio, S. Kraml, S. Kulkarni, U. Laa, A. Lessa, V. Magerl, J. Sonneveld, M. Traub, and W. Waltenberger, *Comput. Phys. Commun.* **227**, 72 (2018), [arXiv:1701.06586 \[hep-ph\]](#).
- [88] F. Ambrogio *et al.*, *Comput. Phys. Commun.* **251**, 106848

- (2020), [arXiv:1811.10624 \[hep-ph\]](#).
- [89] J. Dutta, S. Kraml, A. Lessa, and W. Waltenberger, *LHEP* **1**, 5 (2018), [arXiv:1803.02204 \[hep-ph\]](#).
- [90] A. Buckley, *Eur. Phys. J. C* **75**, 467 (2015), [arXiv:1305.4194 \[hep-ph\]](#).
- [91] T. Sjostrand, S. Mrenna, and P. Z. Skands, *JHEP* **05**, 026 (2006), [arXiv:hep-ph/0603175](#).
- [92] T. Sjöstrand, S. Ask, J. R. Christiansen, R. Corke, N. Desai, P. Ilten, S. Mrenna, S. Prestel, C. O. Rasmussen, and P. Z. Skands, *Comput. Phys. Commun.* **191**, 159 (2015), [arXiv:1410.3012 \[hep-ph\]](#).
- [93] J. Alwall, R. Frederix, S. Frixione, V. Hirschi, F. Maltoni, O. Mattelaer, H. S. Shao, T. Stelzer, P. Torrielli, and M. Zaro, *JHEP* **07**, 079 (2014), [arXiv:1405.0301 \[hep-ph\]](#).
- [94] V. Hirschi and O. Mattelaer, *JHEP* **10**, 146 (2015), [arXiv:1507.00020 \[hep-ph\]](#).
- [95] M. Wiesemann, R. Frederix, S. Frixione, V. Hirschi, F. Maltoni, and P. Torrielli, *JHEP* **02**, 132 (2015), [arXiv:1409.5301 \[hep-ph\]](#).
- [96] R. Harlander, M. Kramer, and M. Schumacher, (2011), [arXiv:1112.3478 \[hep-ph\]](#).